Jin et al. Journal of Wood Science (2024) 70:5
https://doi.org/10.1186/s10086-023-02117-x

Journal of Wood Science

ORIGINAL ARTICLE

Open Access

Determination of nuclear magnetic resonance surface relaxivity for the macropore system from wood cell lumen

Zhi Jin[1], Yuejin Fu[1], Qian Chen[1] and Zhen Zeng[1*]

Abstract

To determine the surface relaxivity of pores plays a vital role in the application of time-domain nuclear magnetic resonance (TD-NMR) technology to porous structure characterization for wood. Currently, the surface relaxivity of pores is calibrated using a standard sample with a pore size of the same order as the wood pore system. However, the uniformly distributed pore size of standard sample is unfit to accurately indicate the complexity of porous structure of wood, which significantly affects the accuracy of test results. By integrating the TD-NMR technology with mercury intrusion porosimetry (MIP), the surface relaxivity of macropores in the lumen of wood cells is calibrated in this study using the tested sample, so as to avoid the error in measurement as caused by existing method. Data processing is performed using several mathematical methods including interpolation arithmetic and least square principle. Notably, the node segmentation method is applied to identify the T_2 boundary of pores in cell lumen and to classify the porous structure of cell lumen into different pore systems. The approach proposed in this study is demonstrated to be effective in improving the accuracy of TD-NMR technology for characterizing the porous structure of wood. Also, it contributes a potential solution to accounting for the porous structure of wood based on the phenomenon of pore relaxation, which can improve the understanding of wood pore conformation.

Keywords Wood pore structure, Nuclear magnetic resonance, Surface relaxivity, Wood cell lumen, Pore size distribution

Introduction

As a renewable type of biomass material with the highest yield and most extensive range of applications in nature, wood possesses a series of advantages in environmental protection, such as high degradability, excellent biocompatibility and low carbon emissions [1, 2]. In general, the hierarchical porous structure of wood can be divided into macropores, mesopores and micropores in the order from large to small. Macropores are derived mainly from the vessel, tracheid, wood fiber and resin canal, while micropores are dominated by the cell wall pores with the magnitude order of molecular chain section as the largest starting point, such as the space in inter-cellulose molecular chain [3]. Mesopores are smaller than macropores but larger than micropores, such as the pit membranes and inter-microfibril space in cell walls [4–6]. Figure 1 illustrates the pores of different sizes in the hierarchical structure of wood [7–10], and Table 1 lists the sizes of pores in the wood of some specific structures [11, 12]. The porous structure of wood is essential for its practical application for two reasons. On the one hand, it affects the quality of wood processed through traditional methods including wood drying, wood impregnation and wood modification [13, 14]. On the other hand, it serves as a crucial carbon skeleton precursor needed to construct biological templates for extensive applications in

*Correspondence:
Zhen Zeng
Z13522948894@163.com
[1] Research Institute of Wood Industry, Chinese Academy of Forestry, Beijing 100091, China

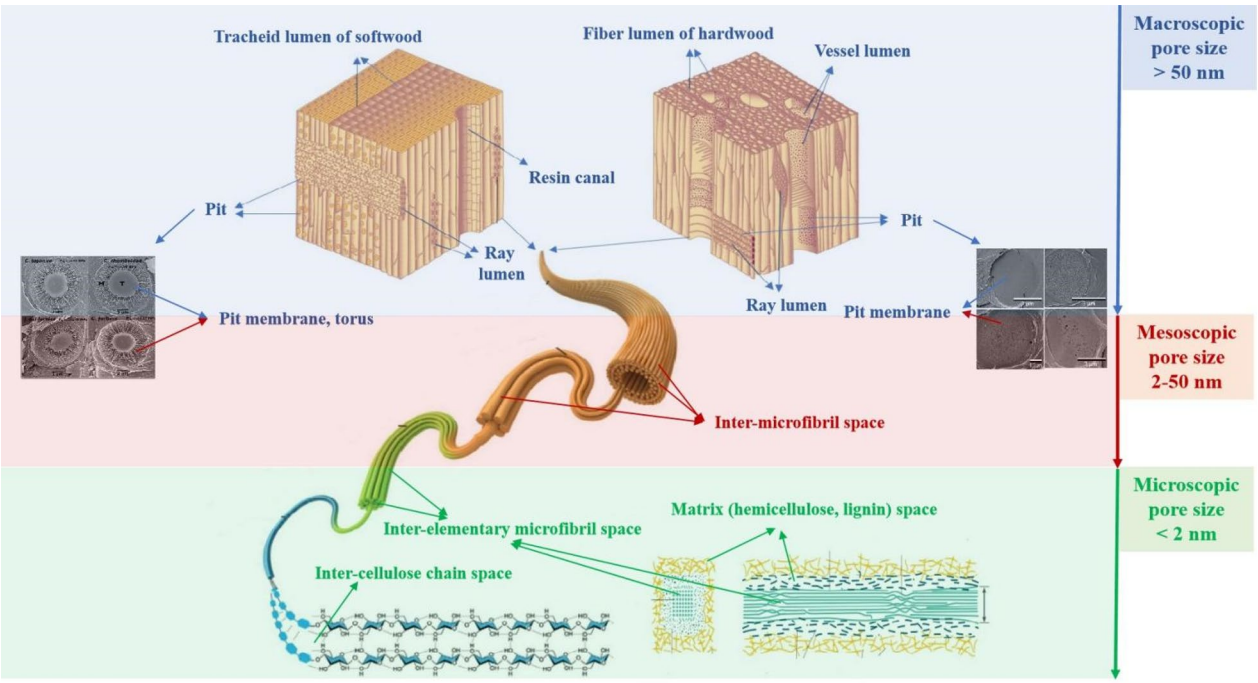

Fig. 1 Pores of different scales in the wood hierarchical structure [7–10]

Table 1 The pore sizes of some specific structural elements in wood [11–13]

Wood species	Structural elements	Pore size	Pore scale
Spruce	Cell wall pores (wetted)	0.4–40 nm	Micro-mesopore
–	Cell wall pores (wetted)	1–10 nm	Micro-mesopore
–	Inter-microfibril spaces	2–4.5 nm	Mesopore
Softwoods	Cell wall pores (dried)	2–100 nm	Meso-macropore
Ring porous hardwoods	Cell wall pores (dried)	2–100 nm	Meso-macropore
Diffuse porous hardwoods	Cell wall pores (dried)	2–100 nm	Meso-macropore
Softwoods	Pit membranes of bordered pits	10 nm-8 μm	Meso-macropore
Softwoods	Pit apertures of bordered pits	400 nm-6 μm	Macropore
Hardwoods	Lumens of fibers	1–30 μm	Macropore
Softwoods	Pit chamber apertures of bordered pits	4–30 μm	Macropore
Hardwoods	Alternate pits	5–170 μm	Macropore
Softwoods	Lumens of tracheid	10–50 μm	Macropore
Ring porous hardwoods	Lumens of vessels	20–400 μm	Macropore
Softwoods	Resin canals	30–300 μm	Macropore
Diffuse porous hardwoods	Lumens of vessels	40–250 μm	Macropore

The microscopic pore size is < 2 nm, mesoscopic pore size is 2–50 nm, and macroscopic pore size is > 50 nm

various innovative fields like oil absorbent [15, 16], sensor [17–19], solar energy evaporator [20–22] and electrochemical catalysis [23–26]. Therefore, it is necessary to collect the information about pore structure thoroughly and accurately for the further development of high-performance wood-based product.

The time-domain nuclear magnetic resonance (TD-NMR) technology provides an advanced and powerful tool for the comprehensive analysis of pores in wood [27, 28]. When radiofrequency pulse is applied to the nuclei in a static magnetic field, the nuclei shift from low energy level to high energy level by absorbing energy from the radiofrequency pulse. After the equilibrium state is

reached, the external radiofrequency pulses are removed, and the nuclei release the absorbed energy to restore the low energy level. During this process, the spin–lattice relaxation, which occurs due to the release of energy from the spinning nuclei to the surroundings, and the spin–spin relaxation, which is caused by energy conversion among the spinning nuclei, complete the relaxation phenomenon. Since the occurrence of relaxation is caused by the interaction among the nuclear spin, the fluid and the pore wall, the TD-NMR signal generated during relaxation carries the information about porous structures. In the TD-NMR method, the relaxation properties of water molecules with ^{1}H protons as probe are measured for the test samples saturated with water, so as to collect the T_2 data of spin–spin relaxation time (i.e., transverse relaxation time) that can be used to reveal the pattern of pore size distribution (PSD). Compared with other commonly used techniques of pore structure characterization, such as gas adsorption isotherms, mercury intrusion porosimetry (MIP), thermoporometry, cryoporometry, microscopic imaging and computed tomography [29], the TD-NMR method shows such advantages as rapidity, non-toxicity and the recyclability of samples. Moreover, there is an extremely wide range of pore sizes that can be detected due to the full penetration of water molecules into various pore systems of different sizes in wood [6, 30].

The linear relationship between T_2 relaxation time and pore diameter is expressed [31–35] as Eq. (1):

$$d = 2\rho_2 F_s T_2, \tag{1}$$

where d represents the pore diameter, ρ_2 indicates the pore surface relaxivity, F_s denotes the pore geometric shape factor, and T_2 stands for the transverse relaxation time. Apparently, to determine the surface relaxivity of pores plays a critical role in the conversion between T_2 distribution and PSD. In the existing studies, the surface relaxivity of pores is calibrated using a standard sample with the pore size of the same order as the wood pore system to be measured for determining the PSD. However, the uniformly distributed pore size of standard samples is unsuited to indicating the complexity of porous structures in wood accurately, which affects the accuracy of test results significantly.

In the present study, a novel approach is developed to determine the NMR surface relaxivity of macropores derived from wood cell lumen. Using the tested wood sample, the surface relaxivity is calibrated, which prevents the measurement error caused by the standardized sample calibration as suggested in the existing methods. Also, the accuracy in characterizing the porous structure of wood is effectively improved by applying the TD-NMR technology.

Materials and methods

Materials

The fir (*Cunninghamia lanceolata*) was obtained from Anhui Province, and the cuboid samples with an approximate size of 10 mm (Tangential) × 10 mm (Radial) × 18 mm (Longitudinal) were obtained by cutting the discs longitudinally and then air dried.

TD-NMR measurement

After being boiled in water bath for 30–60 min, the wood specimens were taken out and immersed in distilled water for 20 days of saturation at room temperature. Afterward, the samples were weighed every 10 days until the difference in water absorption rate between the two adjacent locations fell below 5%. To ensure the smooth saturation of wood, the samples immersed in distilled water were stored in vacuum for 24 h. The final mass m1 and size (length, width and height) of saturated specimens were recorded, whose accuracy reached 0.001 g and 0.01 mm, respectively. After the excess water left on the surface was removed, the water-saturated specimen was transferred into the test tube, with T_2 measured by the TD-NMR (Niumag NMRC12-010 V instrument, Suzhou Niumag Analytical Instrument Corporation, Suzhou, China) with Carr-Purcell-Meiboom-Gill (CPMG) pulse sequence, 90-degree pulse value of 7.4 μs, 180-degree pulse value of 14.8 μs, 16 times of scanning, cycle delay time of 2 s, echo time of 0.15 ms, and echo number of 6000. Finally, it was inversed by SIRT arithmetic [36].

MIP measurement

After TD-NMR test, the above wood specimen was fully dried in an oven at 105 ℃, with the mass m_2 of completely dry specimen recorded. Then, the dried wood specimen was measured using an automatic mercury intrusion porosimeter (AutoPore IV 9500 Version 2.03.00, Micromeritics Instrument Corporation, USA) under the pressure ranging from 0.1 to 61000 PSI at room temperature to determine the porosity and PSD values.

Results and discussion

T_2 distribution analysis

Figure 2 shows the T_2 distribution of the tested wood sample. It can be observed that three peaks denoted as P1 (at 126.04 ms), P2 (at 18.04 ms) and P3 (at 1.70 ms) respectively appear with the extension of T_2 time. The occurrence of relaxation is caused by the relaxation of ^{1}H protons from the water filled with wood pores and the relaxation time is prolonged with the increase of pore size. According to literature [37, 38], the P1

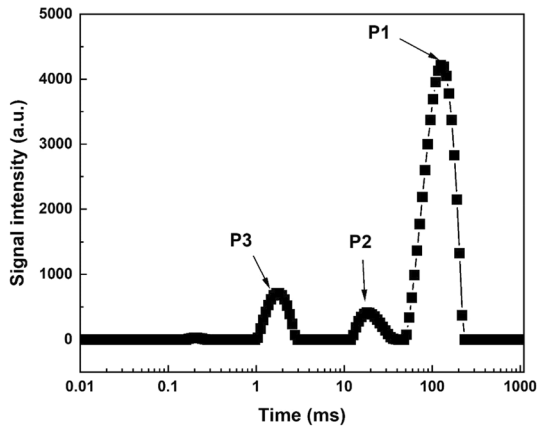

Fig. 2 The T_2 distribution of the tested wood sample

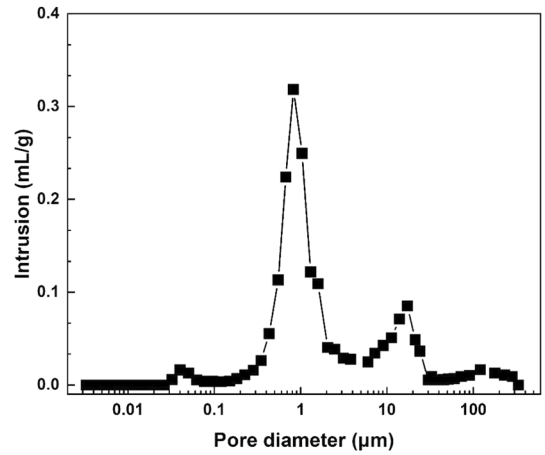

Fig. 3 The PSD of tested wood sample obtained by MIP

and P2 with a longer relaxation time than 10 ms are assigned to the free water contained in macroscopic and mesoscopic pores, such as cell lumen pores, pit and inter-microfibril space. It is also suspected that the water component from P2 is more likely attributed to the water from pits, because the P2 appears to have association with P1 and a shorter relaxation time, suggesting that its water component is connected to the water component derived from P1 and subjected to a tighter restriction in the smaller porous structure [38, 39]. Representing the bound water in the microscopic pores located mainly in the cell wall, P3 is classified into two components, i.e., the water molecules adsorbed through hydrogen bonds to cell wall polymers and the water clusters trapped in small voids [40–42]. In general, the relaxation time of bound water is less than 10 ms, despite some literature indicating that the bound water content as calculated using T_2 data only within 10 ms is unduly low [43]. Thus, it remains necessary to determine the relaxation time boundary between free water and bound water, which is also affected by the boundary of different pore scale systems of water-saturated wood specimens.

MIP PSD analysis

Based on the non-infiltrating properties of liquid mercury, the MIP method is applied to the characterization of porous structure in wood by injecting liquid mercury into wood specimens. Then, the PSD is evaluated according to Washburn equation [44] as shown in Eq. (2):

$$r = -2\gamma\cos\theta/p, \tag{2}$$

where r represents the pore radius, γ indicates the surface tension of mercury (0.48 N/m), θ denotes the wetting angle of mercury (140°), and p stands for the pressure. Figure 3 shows the PSD of tested wood sample as obtained by MIP. As can be seen from the figure, the PSD ranges from 0.03 μm to 282.88 μm with a distinct peak observed at 0.83 μm and a moderate peak discovered at 17.25 μm, which is ascribed mainly to the macroscopic and mesoscopic pore systems in wood. For the characterization of micropores by MIP, the high pressure makes it inevitable to destroy the micropore structure and affect the accuracy of measurement [45].

Determination of ρ_2 for wood cell lumen macropore system

This study aims to determine the relationship between the T_2 relaxation time and MIP pore diameter (d_m) in the cell lumen macropores. Due to the limitation of the MIP method, it is impossible to detect those micropores whose $d_m < 3$ nm, which is not the case for the TD-NMR method. To ensure the consistency and comparability between these two methods, the range of cumulative distribution percentage as used for calculation is supposed to be within the percentage of mercury saturation (P_s), which is calculated using Eq. (3):

$$P_s = P_m/P_n \times 100\% = P_m /[(m_1 - m_2)/(\rho_w \times V)] \times 100\%, \tag{3}$$

where P_m represents the porosity measured using the MIP method, P_n indicates the porosity of water-saturated sample, m_1 denotes the water-saturated sample mass; m_2 refers to the dry sample mass; ρ_w indicates the density of water at room temperature (1 g/cm^3); and V denotes the volume of the saturated sample [46]. According to the experimental data obtained in this study, P_s is 91.01%, which means the range of calculation as required to determine the linear relationship between T_2 relaxation time and d_m is the range in which the cumulative distribution percentage does not exceed 91.01%, as shown in

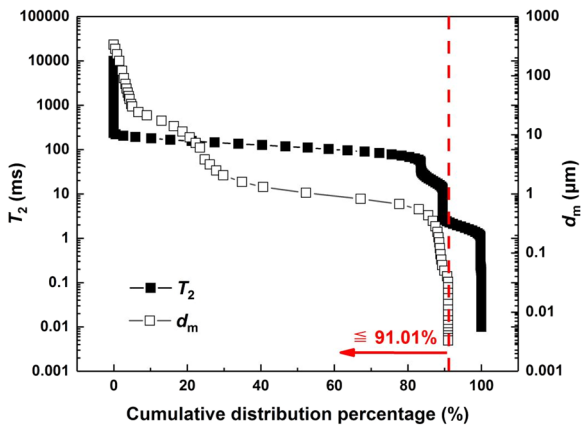

Fig. 4 The cumulative distribution curves of T_2 and d_m

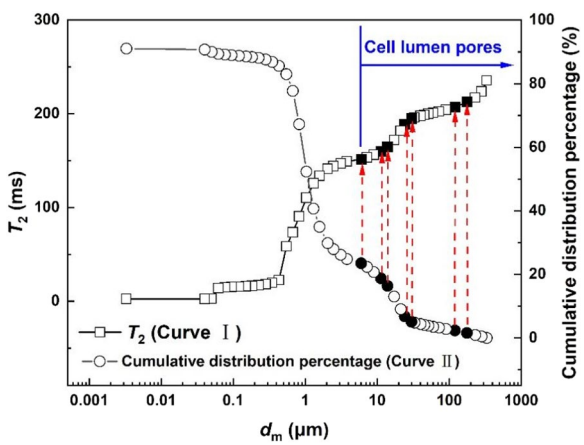

Fig. 5 The correlation between T_2 and d_m (Curve I) and the d_m cumulative distribution (Curve II). The determined nodes of Curve II and their corresponding locations in Curve I pointed by red arrows were shown as filled dots and squares, respectively

Fig. 4. Within the above range, the values of T_2 and d_m are obtained by means of interpolation arithmetic and the correlation between T_2 and d_m is shown in Fig. 5 (Curve I).

The d_m cumulative distribution as shown in Fig. 5 (Curve II) can be treated as a series of straight lines with different slopes, and the data of each consistent slope are obtained from the same pore system with a similar porous structure [47]. Thus, nodes are introduced to locate these multiple pore systems and calculate the transverse coefficients of T_2 and d_m for each cell lumen macropore system separately. Since the wood sample used in this study is classed into the softwood with a greater tracheid diameter than 10 μm [6, 48], the lower limit of the cell lumen pore diameter (d_{min}) is set to the same as the d_m at the end node of the last pore system through the d_m data point which is the closest to 10 μm. Herein, d_{min} = 6.03 μm, and the T_2 is 151.48 ms accordingly. This is consistent with the argument that the T_2 boundary between free water and bound water should be no less than 10 ms [43]. As shown in Fig. 5, the starting and ending nodes of each consistent slope part on Curve II are taken as the nodes for segmentation by filled dots, and the determined nodes are indicated by filled squares on Curve I. The values of these nodes are listed in Table 2.

After the calculation interval is subdivided as above, Eq. 4 is used to quantify the linear relationship between T_2 and the d_m for each cell lumen pore system using the least square method. This is purposed to determine the conversion coefficient K_i for the ith pore system when the error δ_i between the pore size value as calculated by $K_i \times T_{2j}$ and the d_{mj} reaches its minimal. In addition, the pore size distribution percentage w_j is introduced as the weight for calculation, so as to reduce the impact of PSD inhomogeneity on the fitting error [49]. The residual in regression calculation is ignored.

$$\delta_i = \left(\sum_{(j=1)}^{n} w_j (d_{mj} - K_i \times T_{2j})2 / \sum_{(j=1)}^{n} w_j \right)^{1/2} \tag{4}$$

where n represents the number of data points between two adjacent nodes in Curve I; w_j indicates the distribution percentage of the jth d_m data point between two adjacent nodes, and d_{mj} denotes the d_m value of the jth data point between two adjacent nodes; T_{2j} refers to the T_2 value of the jth data point between two adjacent nodes. Based on this, "XIAOXIAOMU WOOD FAIRY" software is developed to calculate the K_i value of different pore systems, the results of which are shown in Table 2. Compared with manual calculation, the software reduces the calculation time for each sample from 3 to 5 h to 5 min, while eliminating the error caused by manual calculation. This significantly improves the efficiency of calculation, and facilitates the large-scale calculation as required for future research.

Table 2 Calculation results of different pore systems

Pore system	d_m (μm)	T_2 (ms)	K_i	ρ_{2i} (μm/ms)
1	≥177.44	≥212.74	1.0352	0.2588
2	120.69–177.44	207.19–212.74	0.6961	0.1740
3	30.15–120.69	194.82–207.19	0.3520	0.0880
4	24.14–30.15	188.71–194.82	0.1316	0.0329
5	13.94–24.14	164.64–188.71	0.1048	0.0262
6	11.33–13.94	160.07–164.64	0.0791	0.0198
7	6.03–11.33	151.48–160.07	0.0573	0.0143
			Average	0.0877

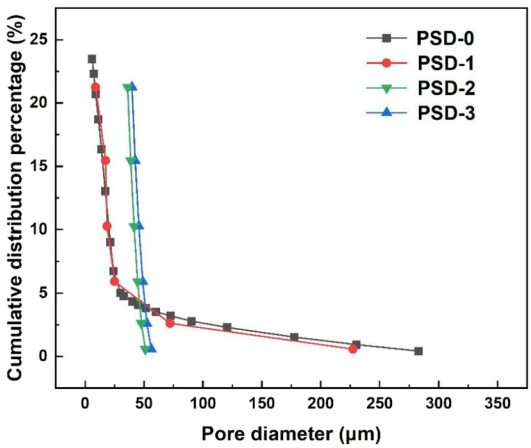

Fig. 6 The comparison in the PSD calculated by different methods

To verify the above method for its accuracy, Fig. 6 compares the PSD experimentally given by the MIP method (PSD-0) with the PSDs estimated from T_2 value using K_i values in Table 2 (PSD-1), K value calculated without introducing nodes (PSD-2), and K value calculated by method mentioned in existing studies (PSD-3). It can be found out that the PSD-1 is more consistent with PSD-0 than both PSD-2 and PSD-3. This confirms the reliability of the approach proposed in this study.

Finally, the surface transverse relaxivity ρ_{2i} is calculated by substituting the K_i values into Eq. (5) as follows:

$$\rho_{2i} = K_i/(2 \times F_s), \tag{5}$$

where $F_s = 2$ since the pore shape is assumed as cylindrical in accordance with the MIP method. Table 2 lists the ρ_{2i} values of different macropore systems derived from wood cell lumen. It can be found out that the calculated ρ_{2i} values are of the same magnitude order with an average of 0.0877 μm/ms obtained through the existing method and standardized sample calibration ($\rho_2 = 0.064$ μm/ms for cell lumen pores and 0.0027 μm/ms for cell wall pores). Meanwhile, the ρ_{2i} value is also calculated to show a decreasing trend with the reduction in pore size. This substantiates the feasibility and effectiveness of the proposed approach.

Conclusion

In the present study, a novel approach is developed to determine the TD-NMR transverse surface relaxivity of the macropore system derived from wood cell lumen. The surface relaxivity of the tested sample is calibrated by integrating TD-NMR with MIP. Also, data processing is conducted according to interpolation arithmetic and least square principle. Then, the node segmentation method is introduced to significantly improve the accuracy of TD-NMR technology for PSD characterization of wood. To sum up, this study contributes a potential solution to accounting for the porous structure of wood based on pore relaxation for the full understanding of wood pore conformation.

Abbreviations

TD-NMR	Time-domain nuclear magnetic resonance
PSD	Pore size distribution
MIP	Mercury intrusion porosimetry

Acknowledgements

This work was supported by the National Natural Science Foundation for Youth (32001254).

Author contributions

ZJ: funding acquisition, conceptualization, methodology, validation, investigation, writing—original draft. YF: conceptualization, methodology, supervision. QC: methodology, writing—review and editing. ZZ: conceptualization, methodology, validation, investigation, writing—review and editing.

Funding

This study was funded by the National Natural Science Foundation for Youth (32001254).

Availability of data and materials

All data generated or analyzed during this study are included in this published article.

Declarations

Competing interests

The authors declare that they have no competing interests.

Received: 11 May 2023 Accepted: 20 December 2023
Published online: 11 January 2024

References

1. Wang ZG, Zhang XF, Ding ML, Yao JF (2022) Aminosilane-modified wood sponge for efficient CO_2 capture. Wood Sci Technol 56(3):691–702
2. Lu Y (2022) Wood supramolecular science: scientific significance and prospects. Chin J Wood Sci Technol 36(2):1–10
3. Sinko R, Mishra S, Ruiz L, Brandis N, Keten S (2017) Dimensions of biological cellulose nanocrystals maximize fracture strength. Acs Macro Lett 3(1):64–69
4. Zhao G (2002) Nano-dimensions in wood, nano-wood, wood and inorganic nano-composites. J Beijing For Univ 24(5):204–207
5. Jin Z, Ma J, Fu Y (2021) Research on the distribution of cell wall components and porosity in populous nigra tension wood fiber based on Raman imaging data. Spectrosc Spect Anal 41(3):801–806
6. Wang Z, Wang X (2014) Research progress of multi-scale pore structure and characterization methods of wood. Scientia Silvae Sinicae 50(10):123–133
7. Chen C, Kuang Y, Zhu S, Burgert I, Keplinger T, Gong A, Li T, Berglund L, Eichhorn S, Hu L (2020) Structure-property-function relationships of natural and engineered wood. Nat Rev Mater 5(09):642–666
8. Chen C, Hu L (2020) Nanoscale ion regulation in wood-based structures and their device applications. Adv Mater 33(28):2002890
9. Li S, Lens F, Espino S, Karimi Z, Klepsch M, Schenk H, Schmitt M, Schuldt B, Jansen S (2016) Intervessel pit membrane thickness as a key determinant of embolism resistance in angiosperm xylem. IAWA J 37(02):152–171
10. Pittermann J, Choat B, Jansen S, Stuart S, Lynn L, Dawson T (2010) The relationships between xylem safety and hydraulic efficiency in the

cupressaceae: the evolution of pit membrane form and function. Plant Physiol 153(04):1919–1931
11. Jin Z, Li B, Yin J, Chen Q, Fu Y, Lv B (2022) Research progress for the evaluation of wood pore connectivity. Scientia Silvae Sinicae 58(5):177–186
12. He S, Xu J, Wu Z, Hu Y (2017) Compare of porous structure of moso bamboo and Pinus sylvestris L. lumber. J Nanjing For Univ 41(2):157–162
13. Redman AL, Bailleres H, Turner I, Perré P (2016) Characterisation of wood-water relationships and transverse anatomy and their relationship to drying degrade. Wood Sci Technol 50(4):739–757
14. Papadopoulos AN, Bikiaris DN, Mitropoulos AC, Kyzas GZ (2019) Nanomaterials and chemical modifications for enhanced key wood properties: a review. Nanomaterials-basel 9(4):607
15. Lu Y, Li J, Zhang Y, Zhong G, Liu B, Wang H (2020) Wood-derived carbon functional materials. Prog Chem 32(7):906–916
16. Guan H, Cheng Z, Wang X (2018) Highly compressible wood sponges with a spring-like lamellar structure as effective and reusable oil absorbents. ACS Nano 12(10):10365–10373
17. Guan H, Meng J, Cheng Z, Wang X (2020) Processing natural wood into a high-performance flexible pressure sensor. ACS Appl Mater Inter 12(41):46357–46365
18. Guan H, Dai X, Ni L, Hu H, Wang X (2021) Highly elastic and fatigue-resistant graphene-wrapped lamellar wood sponges for high-performance piezoresistive sensors. ACS Sustain Chem Eng 9:15267–15277
19. Tang Q, Zou M, Chang L, Guo W (2021) A super-flexible and transparent wood film silver nanowire electrode for optical and capacitive dual-mode sensing wood-based electronic skin. Chem Eng J 430(4):132152
20. Xue G, Liu K, Chen Q, Yang P, Li J, Ding T, Duan J, Qi B, Zhou J (2017) Robust and low-cost flame-treated wood for high-performance solar steam generation. ACS Appl Mater Inter 9(17):15052–15057
21. Chen C, Li Y, Song J, Yang Z, Kuang Y, Hitz E, Jia C, Gong A, Jiang F, Zhu J, Yang B, Xie J, Hu L (2017) Highly flexible and efficient solar steam generation device. Adv Mater 29(30):1701756
22. Wang Z, Yan Y, Shen X, Jin C, Sun Q, Li H (2019) A wood-polypyrrole composite as a photothermal conversion device for solar evaporation enhancement. J Mater Chem A 7(36):20706
23. Chen C, Hu L (2018) Nanocellulose toward advanced energy storage devices: structure and electrochemistry. Acc Chem Res 51(12):3154–3165
24. Chen C, Zhang Y, Li Y, Kuang Y, Song J, Luo W, Wang Y, Yao Y, Pastel G, Xie J, Hu L (2017) Highly conductive, lightweight, low-tortuosity carbon frameworks as ultrathick 3D current collectors. Adv Energy Mater 7(17):1700595
25. Song H, Xu S, Li Y, Dai J, Gong A, Zhu M, Zhu C, Chen C, Chen Y, Yao Y, Liu B, Song J, Pastel G, Hu L (2018) Hierarchically porous, ultrathick, "breathable" wood-derived cathode for lithium-oxygen batteries. Adv Energy Mater 8(4):1701203
26. Lu Y, Lu Y, Jin C, Gao R, Liu B, Huang Y, Yu Y, Ren J, Deng Y, Tao X, Lyu J (2021) Natural wood structure inspires practical lithium-metal batteries. ACS Energy Lett 6(6):2103–2110
27. Guo X, Wu Y, Yan N (2017) Characterizing spatial distribution of the adsorbed water in wood cell wall of Ginkgo biloba L. by μ-FTIR and confocal Raman spectroscopy. Holzforschung 71(5):415–423
28. Gao Y, Xu K, Jiang J, Lyu J (2018) Application of time domain nuclear magnetic resonance technology to wood science research. World For Res 31(5):33–38
29. Wason J, Bouda M, Lee EF, McElrone AJ, Phillips RJ, Shackel KA, Matthews MA, Brodersen C (2021) Xylem network connectivity and embolism spread in grapevine (Vitis vinifera L.). Plant Physiol 186(1):373–387
30. Wen J, Sun S, Xue B, Sun R (2013) Recent advances in characterization of lignin polymer by solution-state nuclear magnetic resonance (NMR) methodology. Materials 6(1):359–391
31. Durrett R (1984) Oriented percolation in two dimensions. Ann Probab 12(4):999–1040
32. Toumelin E, Torres-Verdín C, Sun B, Dunn KJ (2007) Random-walk technique for simulating NMR measurements and 2D NMR maps of porous media with relaxing and permeable boundaries. J Magn Reson 188(1):83–96
33. Li X, Li Y, Chen C, Zhao D, Wang X, Zhao L, Shi H, Ma G, Su Z (2015) Pore size analysis from low field NMR spin-spin relaxation measurements of porous microspheres. J Porous Mat 22(1):11–20
34. He Y, Mao Z, Xiao L, Ren X (2005) An improved method of using NMR T_2 distribution to evaluate pore size distribution. Chin J Geophys 48(2):412–418
35. Li X, Zhao Z (2020) Time domain-NMR studies of average pore size of wood cell walls during drying and moisture adsorption. Wood Sci Technol 54(5):1241–1251
36. Kak AC, Slaney M (1988) Principles of computerized tomographic imaging. IEEE Press, New York
37. Gezici-Koc Erich SJF, Erich HP, Huinink LGJ, van der Ven OCGA (2017) Bound and free water distribution in wood during water uptake and drying as measured by 1D magnetic resonance imaging. Cellulose 24(2):535–553
38. Li J, Ma E, Yang T (2019) Differences between hygroscopicity limit and cell wall saturation investigated by LF-NMR on Southern pine (Pinus spp.). Holzforschung 73(10):911–921
39. Fredriksson M, Thygesen LG (2017) The states of water in Norway spruce [Picea abies (L.) Karst.] studied by low-field nuclear magnetic resonance (LFNMR) relaxometry: assignment of free-water populations based on quantitative wood anatomy. Holzforschung 71(1):77–90
40. Cox J, Mcdonald PJ, Gardiner BA (2010) A study of water exchange in wood by means of 2D NMR relaxation correlation and exchange. Holzforschung 64(2):259–266
41. Bonnet M, Courtier-Murias D, Faure P, Rodts S, Care S (2017) NMR determination of sorption isotherms in earlywood and latewood of Douglas fir. Identification of bound water components related to their local environment. Holzforschung 71(6):481–490
42. Jeoh T, Karuna N, Weiss ND, Thygesen LG (2017) Two dimensional ^{1}H-nuclear magnetic resonance relaxometry for understanding biomass recalcitrance. ACS Sustain Chem Eng 5:8785–8795
43. Gao X, Cai J, Jin J, Zhuang S (2017) Bound water content and pore size diameter distribution in swollen cell walls determined by NMR cryoporometry. J Nanjing For Univ 41(2):7
44. Washburn EW (1921) Note on a method of determining the distribution of pore sizes in a porous material. P Natl Acad Sci USA 7(4):115–116
45. Zhao J, Yang L, Cai Y (2021) Combining mercury intrusion porosimetry and fractal theory to determine the porous characteristics of wood. Wood Sci Technol 55(1):109–124
46. Li A, Ren X, Wang G, Wang Y, Jiang K (2015) Characterization of pore structure of low permeability reservoirs using a nuclear magnetic resonance method. J Chin Univ Petroleum 39(6):92–98
47. Han Y, Zhang C, Zhang Z, Zhang H, Chen L (2019) Pore structure classification and logging evaluation method for carbonate reservoirs: a case study from an oilfield in the Middle East. Energy Source Part A 41(13–18):1701–1715
48. He S, Chen Y, Wu Z, Hu Y (2018) Research progress on wood/bamboo microscopic fluid transportation. Chin For Sci Technol 5(2):12–19
49. Li H, Li J, Guo H (2008) Methods for calculating pore radius distribution in rock from NMR T_2 spectra. Chin J Magnetic Resonance 25(2):273–280

Publisher's Note